Biol. Cybern. (2003)
DOI 10.1007/s00422-003-0430-i

Biological Cybernetics

Conduction in bundles of demyelinated nerve fibers: computer simulation

S. Reutskiy[1], **E. Rossoni**[2], **B. Tirozzi**[2]

[1] Magnetohydrodynamics Laboratory, P.O. Box 136, Moskovski Ave., 199, 61037, Kharkov, Ukraine
[2] Physics Department, University of Rome "La Sapienza", P-le A. Moro 2, 00185, Rome, Italy

Received: 9 December 2002 / Accepted: 30 July 2003 / Published online: ■

Abstract. This study presents a model of action potential propagation in bundles of myelinated nerve fibers. The model combines the single-cable formulation of Goldman and Albus (1967) with a basic representation of the ephaptic interaction among the fibers. We analyze first the behavior of the conduction velocity (CV) under the change of the various conductance parameters and temperature. The main parameter influencing the CV is the fast sodium conductance, and the dependence of CV on the temperature is linear up to 30 °C. The increase of myelin thickness above its normal value (5 μm) gives a slight increase in CV. The CV of the single fiber decreases monotonically with the disruption of myelin, but the breakdown is abrupt. There is always conduction until the thickness is larger than 2% of its original value, at which point a sharp transition of CV to zero occurs. Also, the increase of temperature can block conduction. At 5% of the original thickness there is still spike propagation, but an increase of 2 °C causes conduction block. These results are consistent with clinical observations. Computer simulations are performed to show how the CV is affected by local damage to the myelin sheath, temperature alterations, and increased ephaptic coupling (i.e., coupling of electrical origin due to the electric neutrality of all the nerve) in the case of fiber bundles. The ephaptic interaction is included in the model. Synchronous impulse transmission and the formation of "condensed" pulse states are found. Electric impulses with a delay of 0.5 ms are presented to the system, and the numerical results show that, for increasing coupling, the impulses tend to adjust their speed and become synchronized. Other interesting phenomena are that spurious spikes are likely to be generated when ephaptic interaction is raised and that damaged axons suffering conduction block can be brought into conduction by the normal functioning fibers surrounding them. This is seen also in the case of a large number of fibers ($N = 500$). When all the fibers are stimulated simultaneously, the conduction velocity is found to be strongly dependent on the level of ephaptic coupling and a sensible reduction is observed with respect to the propagation along an isolated axon even for low coupling level. As in the case of three fibers, spikes tend to lock and form collective impulses that propagate slowly in the nerve. On the other hand, if only 10% of fibers are stimulated by an external input, the conduction velocity is only 2% less than that along a single axon. We found a threshold value for the ephaptic coupling such that for lower values it is impossible to recruit the damaged fibers into conduction, for values of the coupling equal to this threshold only one fiber can be restored by the nondamaged fibers, and for values larger than the threshold an increasing number of fibers can return to normal functioning. We get values of the ephaptic coupling such that 25% of axons can be damaged without change of the collective conduction.

1 Introduction

Loss of myelin sheath along tracts of central axons is observed in Multiple Sclerosis (MS), the most common demyelinating disease of the central nervous system in humans (for a complete review of its pathophysiology see Smith and McDonald 1999). The lesions of MS typically arise within the optic nerves, spinal cord, brainstem, and periventricular white matter of the cerebral hemispheres. Many MS symptoms can be explained in terms of conduction deficits in the relevant pathways and directly correlate with loss of myelin. The most dramatic effect of myelin disruption is the conduction block at the site of lesion; segmental demyelination, i.e., loss of a whole internodal sheath, has proven a sufficient condition to produce such an effect. However, depending on the magnitude of demyelination, fibers can partially maintain their ability to conduct impulses.

It has been experimentally demonstrated that demyelinated axons may become hyperexcitable and

Correspondence to: B. Tirozzi
(e-mail: tirozzi@krishna.phys.uniroma1.it,
Tel.: 39-06-49914310, Fax: 39-06-4454749)

4 2 2 | Journal number | 0 4 3 0 | Manuscript number | B
Dispatch: 19.11.2003 | Journal: B C Y B | No. of pages: 10
Author's disk received ☑ Used ☑ | Corrupted ☐ | Mismatch ☐ | Keyed ☐

acquire the property of spontaneously generating trains of spurious impulses (Smith and McDonald 1980, 1982; Baker and Bostock 1992). Moreover, since fibers are often found to lie in closely packed fasces (as in the peripheral nerve bundles, the spinal column, the optic nerves, the cerebellum, and the corpus callosum), lateral spread of excitability via "ephaptic" interaction could lead to an abnormal axon–axon cross talk among adjacent demyelinated fibers and eventually trigger firing in ectopic (i.e., out of place) sites. Though yet to be proven experimentally, this is an intriguing hypothesis that could lead to an explanation of some complicated paroxysmal phenomena observed in MS patients (Matthews 1975).

Since the pioneer work of Hodgkin and Huxley (1952), neural models have proven their utility in delineating the biophysical basis of conduction in nerve fibers. In this study, a computational model of impulse propagation in bundles of myelinated axons is developed in order to help understand the origin of some MS symptoms. The model is based on the Goldman and Albus mathematical description of a myelinated nerve fiber (Goldman and Albus 1968) and accounts for the ephaptic interaction among the axons, following the work of Markin (1970a, b). Though the Goldman and Albus model largely simplifies the description of the axonal membrane under the myelin sheath, it still provides a good quantitative approximation of the electrical behavior of a myelinated fiber, unless total demyelination is considered. Moreover, it is less computationally demanding than the more up-to-date "multicable" models (see, e.g., Nygren and Halter 1999), and therefore it is more suitable for simulating a large ensemble of interacting fibers.

In the following, we will first consider the case of an isolated fiber subjected to segmental demyelination and show how the conduction velocity depends on temperature. Second, we will consider a small bundle of fibers to show how ephaptic interactions can lead to synchronous transmission of impulses and also to the generation of spurious spikes. Finally, we will analyze the case of a large ensemble of interacting fibers and show how coupling can prevent conduction failure. The results of our work are consistent with those of other papers and in some cases confirm and improve their conclusions. We find explicitly spikes induced by ephaptic interaction between neighboring axons, and this result may explain the influence of abnormal ephaptic interaction on membranes with altered excitability. This problem was mentioned in an earlier paper (Waxman 1977) together with the effect of temperature increase on MS symptoms. We do not analyze the structure of the internodal membrane that is under the myelin sheath. However, this simplification has allowed us to study the case of more axons interacting together and to reveal the presence of induced spikes in high ephaptic interaction. The model used by Brill et al. (1977) is similar to our model, but the object of their study is different since they have considered the dependence of spike propagation on the change of internodal length. We did not address this issue, but our model can be used for studying such a dependence and also could generalize this study to the case of interacting fibers. It could be interesting to examine what happens when the internodal length is randomly distributed among different fibers. In this case we cannot use the symmetry among fibers as we did in our case, and the problem could be examined only in the case of a limited number of fibers. Finally, Tuckwell (1993) considered the stationary case of membrane potential and was able to find the distribution of membrane potential from soma to synaptic terminals as a function of myelin thickness. In that work, the explicit solutions of the electric potential are given, but it is not possible to derive the fall of the velocity of propagation of spikes. The latter has been found here by solving numerically the nonstationary case. The same paper considers another situation (soma and terminals), while we consider propagation in axons also interacting among them. It is interesting in any case that we have drawn similar conclusions about the effect of myelin erosion on the propagation of electric potentials in membranes in two different situations.

2 Methods

2.1 Main assumptions

The main assumptions of the model are: (a) the axon is axis symmetric, (b) the inner cross section of the fiber is constant, and (c) the Ranvier nodes are equally spaced.

The first two assumptions are valid for most of the axonal length with the exception of a small region situated around the Ranvier nodes, where the cross section of the axon is reduced and the neuronal membrane assumes a complex shape. The last assumption is correct as long as normal, or recently demyelinated, fibers are considered.

In the "single-cable" model of Goldman and Albus, the structure of the axon is simplified by considering the myelin sheath to be collapsed onto the internodal membrane (see, e.g., Smith and Koles 1970; Waxman and Brill 1978; Stephanova 1989), thus neglecting the so-called *periaxonal* space underneath the myelin. Following this approach, we shall further assume that (d) active ionic currents are concentrated in the Ranvier node, (e) the internodal membrane is totally passive, (f) axon cross sections are isopotential, and (g) ion concentrations are constant.

Assumption (f) is the so-called core-conductor approximation, which is common to a large class of axonal models and allows the system to be treated as one-dimensional. Thus we shall consider only two possible current pathways: longitudinal (along the axoplasm i.e., the internal part of the axon) and transversal (across the membrane). Assumption (g) is a reasonable approximation unless repetitive firing over a long time period is considered because of the low ionic flow.

The last four assumptions simplify the mathematical description of the ephaptic interaction when a bundle of axons is considered: (h) the fibers are parallel and the Ranvier nodes are aligned, (i) all the fibers are identical,

(j) the nerve boundary is perfectly insulating, and (k) each transverse section of the extracellular space is isopotential.

Assumption (h) is considered as a starting point in many theoretical studies based on the observation that axons in a nerve run parallel far from bifurcation. On the other hand, the real degree of nodal alignment is largely unknown and may depend on the specific nerve under consideration; therefore, the simplifying assumption of perfect alignment has been made.

The assumption made in (i) is due to the lack of data on the distribution of the axonal diameters, but it is not essential for the development of the model. Note that this assumption is not connected with the myelin sheath thickness, which can still differ for different fibers and for different parts of the same fiber.

Assumption (j) represents a good approximation, given the low conductivity of the connective tissue enclosing bundles of fibers in a nerve.

The last assumption, (k), is equivalent to considering the transversal extracellular resistance with respect to the longitudinal resistance as negligible; this is reasonable when the axons are closely packed (for an estimate of the extracellular resistance in a model of bundled axons, see Bokil et al. 2001).

2.2 Formulation of the model

Figures 1 and 2 depict an axon and a bundle of axons, respectively, as they are schematized in the model. Let $\phi_k, k = 1, \ldots, N$ and ϕ_0 be the potentials of the fibers and of the interfiber medium, respectively. Under assumption (n) these are functions of the longitudinal coordinate x and time t only.

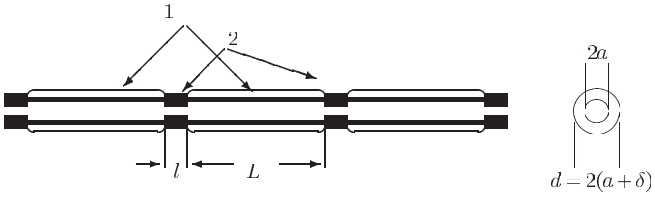

Fig. 1. Sketch of the axon geometry. (1) Myelin sheath. (2) Ranvier nodes (not to scale)

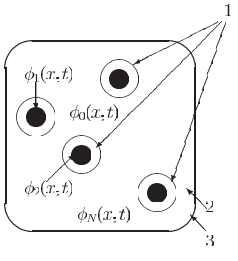

Fig. 2. Schematic drawing of a nerve bundle cross section. (1) Myelinated fibers. (2) Extracellular medium. (3) Low conducting perinerium (not to scale)

From (j) it can be assumed that the system of fibers in the bundle is electrically isolated from the external environment, so the equation

$$I_0(x,t) + \sum_{k=1}^{N} I_k(x,t) = 0 \tag{1}$$

holds, where $I_k(x,t)$ and $I_0(x,t)$ are longitudinal currents in the k-th fiber and in the interfiber medium, respectively. The currents in Eq. 1 are connected to the potentials by Ohm's law:

$$\frac{\partial \phi_0}{\partial x} = -r_0 I_0, \qquad \frac{\partial \phi_k}{\partial x} = -r_f I_k, \qquad k = 1, \ldots, N, \tag{2}$$

where r_0 and r_f are the differential resistances of the interfiber medium and of the k-th fiber, respectively. Note that, according to assumptions (b) and (h), $r_f = const$ and does not depend on which fiber is considered.

We introduce the voltage across either the nodal membrane or the myelin sheath of the k-th fiber as

$$V_k(x,t) = \phi_k(x,t) - \phi_0(x,t). \tag{3}$$

From Eq. 2 it follows that

$$\frac{\partial V_k}{\partial x} = -r_f I_k + r_0 I_0, \quad k = 1, \ldots, N. \tag{4}$$

Using Eq. 1 we obtain

$$I_k = -\frac{1}{r_f}\frac{\partial V_k}{\partial x} + \frac{\alpha_N}{r_f}\sum_{n=1}^{N}\frac{\partial V_n}{\partial x}, \tag{5}$$

where

$$\alpha_N = \frac{\alpha_0}{1 + N\alpha_0}, \quad \alpha_0 = \frac{r_0}{r_f}. \tag{6}$$

On the right-hand side of Eq. 5 the first term represents the longitudinal current along a single axon, while the coupling term

$$I_{\text{eph}}(V_1, \ldots, V_N) = -\frac{\alpha_N}{r_f}\sum_{n=1}^{N}\frac{\partial V_n}{\partial x} \tag{7}$$

represents the *ephaptic* current caused by the electrical interaction between the fibers. The coupling strength α_N depends on the area S_{free}, on the specific resistivity of the extracellular space ρ_0, on the corresponding parameters s and ρ_{ax} of the single fiber, through the expression

$$\alpha_0 = \beta\frac{s}{S_{\text{free}}}, \quad \text{where } \beta = \frac{\rho_0}{\rho_{\text{ax}}}. \tag{8}$$

The ephaptic current is included in the current balance together with the capacitance current, the leakage current, and the ionic current. This produces the membrane equation for the internodal region

$$c_{m,k}(x)\frac{\partial V_k}{\partial t} = \frac{1}{r_f}\frac{\partial^2 V_k}{\partial x^2} + \frac{\partial I_{\text{eph}}(V_1, \ldots, V_N)}{\partial x} - g_{m,k}(x)V_k,$$
$$k = 1, \ldots, N, \tag{9}$$

where $c_{m,k}(x)$ and $g_{m,k}(x)$ are the capacitance and leakage conductance of the myelin sheath per unit length. Following Goldman and Albus (1968), these functions are given in the form

$$c_{m,k}(x) = k_1 \ln^{-1}(D_k(x)/d), g_{m,k}(x) = \frac{1}{k_2}\ln^{-1}(D_k(x)/d), \quad (10)$$

where

$$D_k(x) = d + 2\delta_k(x)$$

s the variable diameter of the k-th fiber, $\delta_k(x)$ is the thickness of the myelin layer at point x, and k_1 and k_2 are constants.

The membrane equations for the Ranvier nodes are produced in a similar way:

$$c_{nd}\frac{\partial V_k}{\partial t} = \frac{1}{r_f}\frac{\partial^2 V_k}{\partial x^2} + \frac{\partial I_{\text{eph}}(V_1,\ldots,V_N)}{\partial x} - j_{\text{ion,k}}(V_k,x,t) - j_{\text{ex,k}}(x,t), \quad k = 1,\ldots,N, \quad (11)$$

where c_{nd} is the nodal capacitance per unit length, j_{ion} the ionic current per unit length, and j_{ex} the stimulating external current per unit length.

The ionic current per unit length is

$$j_{\text{ion}}(V,x,t) = \pi d J_{FH}(V,x,t),$$

where $J_{FH}(V,x,t) = J_K + J_{Na} + J_l + J_p$ is the membrane current density as described by Frankenhaeuser and Huxley (1964):

$$J_K = P_K n^2 Z(K), \quad J_{Na} = P_{Na} m^2 h Z(Na),$$
$$J_p = P_p p^2 Z(Na), \quad J_l = g_l(V - V_l)$$

and

$$Z(Y) = \gamma F E \frac{[Y]_0 - [Y]_i \exp(\gamma E)}{\exp(\gamma E) - 1}, \quad Y = K,\ Na$$

$E = V + V_{\text{rest}}$, $V_{\text{rest}} = -70\,\text{mV}$ is the resting potential, and $\gamma = F/RT$, where T is the absolute temperature, $F = 96487\,\text{K/M}$ the Faraday constant, and R the gas constant.

The term J_p represents a nonspecific (mainly sodium) current, while J_l accounts for the leakage through the nodal membrane. The ionic concentrations inside the axons, $[\cdot]_i$, and in the extracellular space, $[\cdot]_o$, are considered constant.

The time evolution of the activation and inactivation variables is controlled by the following ordinary differential equation:

$$dy/dt = \left[\alpha_y(1-y) - \beta_y y\right] \cdot Q_{10}(T), \quad \text{for } y = m,n,h,p, \quad (12)$$

where the factor $Q_{10}(T) = 3^{(T-20)/10}$, for T in degrees Celsius, accounts for the temperature dependence. The rate functions α and β are given by

$$\alpha_m, \alpha_n, \alpha_p = \frac{A(V-B)}{1 - \exp[(B-V)/C]}$$
$$\alpha_h, \beta_m, \beta_n, \beta_p = \frac{A(B-V)}{1 - \exp[(V-B)/C]}$$
$$\beta_h = \frac{A}{1 + \exp[(B-V)/C]}$$

with the values of A, B, and C given in Table 1. The values of all the other constants are reported in Table 2.

The resulting differential system was integrated numerically by the finite difference method applied in both space and time (see Appendix for details).

3 Results

3.1 Propagation in an isolated fiber

As a general test of the model, we performed an initial series of simulations of an isolated axon approximately 6 cm long, with 30 internodes. For the numerical discretization, ten segments were used to represent each internode, and the time step size was fixed at 0.5 μs. The right end of the fiber was shorted to ground and a symmetry condition imposed at the first Ranvier node. The fiber was considered at resting potential at time $t = 0$. The fiber was stimulated at time $t = 0$ by a pulse current injected at the leftmost Ranvier node (duration 0.01 ms, amplitude 4 nA). The control temperature was fixed at $T = 24\,^{\circ}\text{C}$. Conduction velocity (CV) was inferred from conduction delay taken as the difference in times at which the rising phase of the impulse crossed 70 mV at two selected nodes near the ends of the fiber.

The simulations show a spike to be triggered at the first node, which propagates down the fiber without attenuation (Fig. 3). Action potential characteristics are in agreement with experimental data reported in Frankenhaeuser and Huxley (1964). Simulated spikes showed the presence of a slight hyperpolarising after-potential and no depolarising after-potential. The computed value of CV is 23.07 m/s, in accordance with measured CV on frog motor axons (Tasaki 1953).

A sensitivity analysis revealed that CV has a minor dependence on the nodal parameters, and the variations in CV ranged around ±20% for a relative change of ±50% in ion permeabilities and nodal capacity.

Table 1.

	A (ms^{-1})	B (mV)	C (mV)
α_m	0.36	22	3
β_m	0.4	13	20
α_h	0.1	−10	6
β_h	4.5	45	10
α_n	0.02	35	10
β_n	0.05	10	10
α_p	0.006	40	10
β_p	0.09	−25	20

Table 2.

Symbol	Description	Value	Units	Ref.
d	Axon diameter (bare)	10	μm	[23]
D	Axon diameter (myelinated)	15	μm	″
l	Nodal length	2.5	μm	″
L	Internode length	2000	μm	″
ρ_{ax}	Axoplasmic resistivity	100	Ω cm	″
c_m	Myelin capacitance p.u.a.	18.7	PF cm^{-1}	″
g_m	Myelin conductance p.u.a.	5.6	nS cm^{-1}	″
c_{nd}	Nodal capacitance	1	μF cm^2	″
P_{Na}	Max. Na, f channel permeability	0.008	cm s^{-1}	[5]
P_p	Max. Na, p channel permeability	0.00054	cm s^{-1}	″
P_K	Max. K channel permeability	0.0012	Cm s^{-1}	″
g_L	Leakage-specific conductance	30.3	mS cm^{-2}	″
V_L	Leakage potential	−0.026	MV	″
$[Na]_o$	External Na^+ concentration	114.5	MM	″
$[Na]_i$	Internal Na^+ concentration	13.74	MM	″
$[K]_o$	External K^+ concentration	2.5	MM	″
$[K]_i$	Internal K^+ concentration	120	MM	″
k_1	–	16	pF cm^{-1}	[6]
k_2	–	29	MΩ cm	″

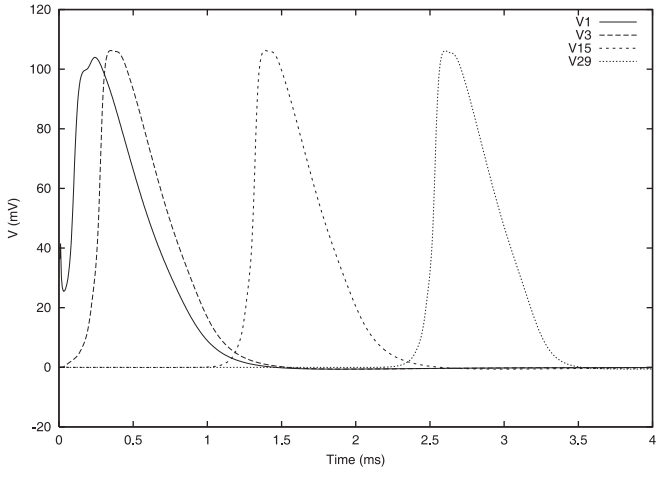

Fig. 3. Test of the single-fiber model. Propagation of action potentials in an isolated normal fiber. The fiber is stimulated at $t = 0$ by a squared pulse current injected at the leftmost Ranvier node. The duration of the stimulus is 0.01 ms and the amplitude is 4 nA. The control temperature is $T = 24\,^{\circ}C$. The spike is triggered at the first node and propagates through the fiber. The computed time course of the membrane potential is plotted at Ranvier nodes 1, 3, 15, 29. The nodal membrane shows an after-hyperpolarization of less than 1 mV and the absence of a depolarizing after-potential. The conduction velocity (CV) is 23.07 m/s, a value equal to the velocity of the propagation of spikes in the frog motor axons (Tasaki 1953). CV ranged 20% around its value for a 50% change in the nodal ion permeabilities and capacity. The fast sodium channel conductance is the most relevant factor controlling fiber excitability and CV. Potassium and persistent sodium channel permeabilities are much less important. The myelin sheath is 5 μm, and its thickening induces a small increase in CV. The dependence of CV on temperature is linear up to 30 °C

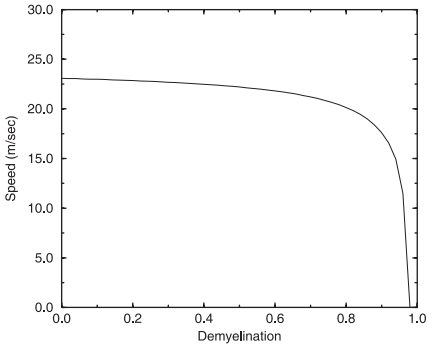

Fig. 4. A fiber approximately 6 cm long with 30 internodes is considered. Each internode is divided into ten equal segments for the discretization procedure. The time step is 0.5 μs. The right-hand side has a potential equal to zero, and a symmetry condition is imposed at the first Ranvier node. The potential is set to its resting value at the initial time. In the picture we plot the computed conduction velocity for a segmentally demyelinated fiber. Myelin sheath thickness is reduced uniformly between nodes 5 and 6, the demyelination ratio, r, being reported in abscissa. An abrupt decrease of the conduction speed takes place when the fiber is severely damaged ($r > 0.8$). Even for a demyelination of about 80% of the initial thickness there is only a 13% decrease in CV and only when the myelin is reduced to less than 2% of its original value is the impulse blocked

Among these parameters, fast sodium channel conductance was found to be the most relevant factor controlling fiber excitability and CV. Potassium and persistent sodium channel permeabilities affected CV by a maximum of 0.5%. CV is inversely proportional to axoplasmic resistivity and is doubled by halving this parameter. Thickening of the myelin sheath results in a slight increase in CV (<10%), suggesting that the fiber setup is near optimum. Temperature dependence was nearly linear up to 30 °C.

The effect of progressive myelin disruption along an entire internode (*segmental demyelination*) was considered by uniformly reducing myelin thickness between nodes 5 and 6. The fractional demyelination was measured by the parameter $r = 1 - \delta/\delta_0$, where δ_0 and δ are the normal and actual thickness of myelination, respectively.

CV is shown to decrease monotonically with disruption of myelin (Fig. 4) because of the capacitive loading of the damaged internode and the consequent

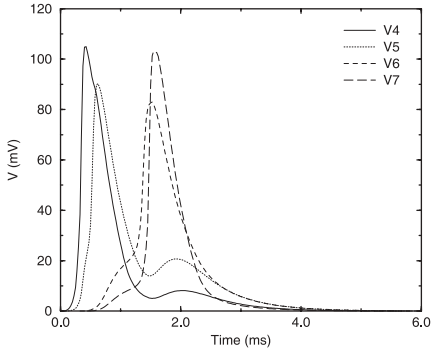

Fig. 5. Computed action potentials around the demyelinated internode, for the case $r = 0.96$. The increased leakage through the damaged internodal membrane reduces the longitudinal current flowing to node 6 and delays the spike onset. After the corrupted tract, the action potential recovers its normal shape and speed. The spike propagation is slowed down from the increased leakage current, but there is no conduction block that takes place abruptly for $r > 0.98$. In the picture, the time evolution of the membrane potential at nodes $4, 5, 6, 7$ is shown. The damaged segment is between nodes 5 and 6

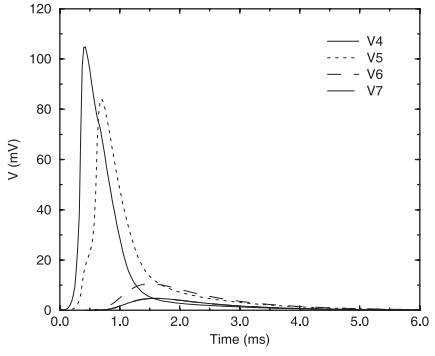

Fig. 6. Computed action potentials around the demyelinated internode, i.e., in the nodes around the damaged area between nodes 5 and 6, for the case $r = 0.98$. The longitudinal current flowing to node 6 is not enough to depolarize the nodal membrane up to the threshold for spike generation, and the impulse conduction is blocked

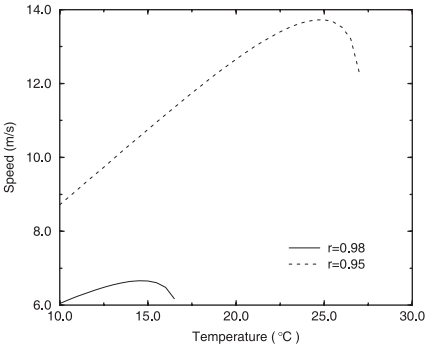

Fig. 7. Calculated temperature dependence of conduction velocity on a segmentally demyelinated fiber. The conduction breakdown occurs at different temperature values, depending on the severity of the demyelination. Although seriously damaged ($r = 0.95$), a fiber can still conduct at control temperature ($T = 24\,^{\circ}\mathrm{C}$) but is blocked by raising the temperature of two degrees. Slow conduction can be restored in a blocked fiber ($r = 0.95$) by lowering the temperature back down to $16\,^{\circ}\mathrm{C}$. This result is consistent with clinical observations. The patients show an increase in symptoms if the temperature rises. Unfortunately, the estimated restoring temperature is too low for clinical therapy

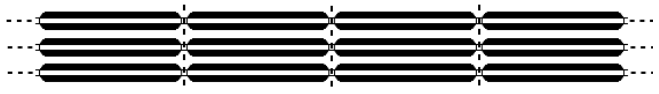

Fig. 8. Schematic drawing of a fascicle of three myelinated fibers (longitudinal section, not to scale). In the bundle model, undamaged fibers are considered to be identical and the Ranvier nodes perfectly aligned. The fibers are one-dimensional and parallel. Before starting the damage, all the internodes have the same myelin thickness, $\delta_0 = 5\,\mu\mathrm{m}$

delay of spike regeneration at node 6 (Fig. 5). The conduction breakdown is abrupt: even for 80% demyelination, only a 13% reduction of the average conduction velocity is observed, so the overall conduction is preserved until severe disruption occurs. For $r > 0.98$ the current leakage from the damaged internode is such that the potential at node 6 cannot reach the threshold to elicit a spike, and the impulse conduction is blocked (Fig. 6).

The temperature dependence was investigated with two levels of demyelination. The results are reported in Fig. 7 and show that a fiber that still conducts at control condition ($r = 0.95$) can be blocked by raising the temperature by $2\,^{\circ}\mathrm{C}$. This result is consistent with clinical observation that patients experienced a worsening of their symptoms after an increase in body temperature (Smith and McDonald 1999). The conduction can be partially restored in a blocked fiber ($r = 0.98$) by lowering the temperature back down to $16\,^{\circ}\mathrm{C}$.

3.2 Propagation in a fiber bundle

Initially we examined the case of $N = 3$ identical fibers bundled together in a small fascicle (Fig. 8). The nerve cross section S was considered as a simulation parameter in order to vary the packing ratio $\gamma = S_{\mathrm{free}}/S$, where S_{free} is the cross section of the extracellular space. The fibers were stimulated with a delay of 0.5 ms, and the spike propagation was traced by recording the earliest times for which the membrane potential in the Ranvier nodes exceeded 70 mV. The results show that for increasing coupling the impulses tend to adjust their speed and become synchronized (Figs. 9 and 10). The impulses markedly slow down once they synchronize. This is

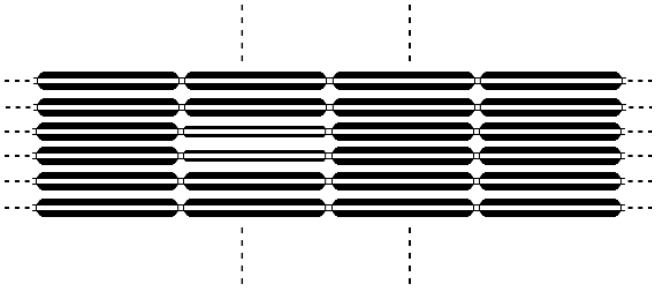

Fig. 9. Impulse propagation in a bundle of three identical axons. The times for which the action potentials are triggered in the Ranvier nodes of each fiber are plotted vs. the node number. A packing ratio of $\gamma = 0.25$ is considered for this case. The packing ratio is inversely proportional to the ephaptic interaction: the more densely the fibers are packed, the larger the interaction strength. The fibers are stimulated with a delay of 0.5 ms, but the propagating action potentials tend to synchronize as they proceed along the axons. The conduction velocity is proportional to the inverse of the slope of the lines in the graphs since the time is displayed on the vertical axis. So

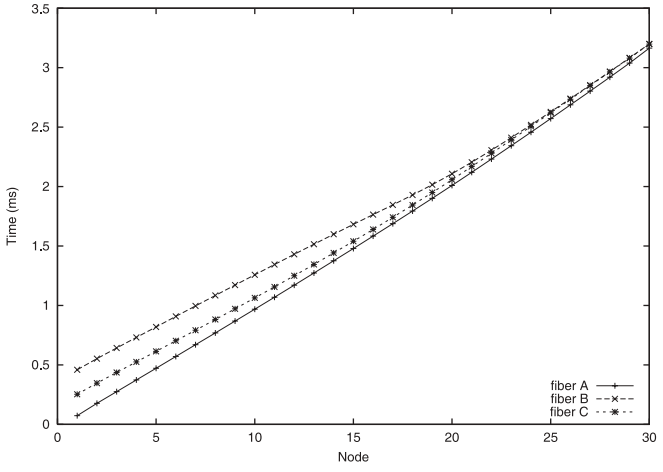

Fig. 10. Impulse propagation in a bundle of three axons ($\gamma = 0.1$); the three fibers (A, B, C) are stimulated as in Fig. 9. Increased coupling ratio produces a faster synchronization: the three propagating action potentials lock together after the first ten nodes. At lower values of γ, i.e., higher values of α, the effect of the decrease of CV of synchronized pulses is more marked

evident from the plot of Fig. 10, where a sudden change in the slope of the time trace is seen after impulse locking.

To better illustrate this phenomenon, the last simulation is repeated by stimulating only two fibers out of three (Fig. 11). In this case, while the impulses in the stimulated fibers (A and B) attract each other to lock together, the ephaptic current induces only a subthreshold wave in the unstimulated fiber (C). As soon as the "coupled pulse" is formed, the ephaptic current increases and finally elicits a "spurious" spike in a Ranvier node of fiber C. Two propagating action potentials arise from this node that move in opposite directions: an antidromic (i.e., backpropagating) spike

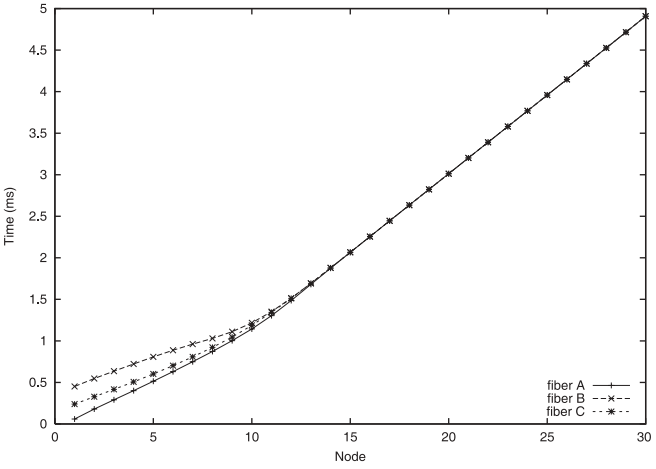

Fig. 11. Impulse propagation in a bundle of three axons ($\gamma = 0.1$). In this case only fibers A and B have been externally stimulated with a delay of 0.5 ms. Fiber C is cross excited at node 24 by the coupled pulses propagating along the other two fibers. As this node is excited, two spurious impulses arise that propagate in opposite directions. The CV reduces each time a new spike is locked with the previous ones

and an orthodromic (i.e., forward) propagating spike, which rapidly synchronizes with the A–B pulse. Note that the collective pulse slows down each time a new action potential is locked to it.

Next, the effects of ephaptic coupling on a large number of fibers were analyzed. To this end we considered a system of $N = 500$ axons enclosed in a nerve of radius $R = 250\,\mu\text{m}$ with a fixed packing ratio of $\gamma \sim 0.65$. In this case the coupling strength was regulated by varying the extracellular resistivity in the range

$$1 < \beta = \frac{\rho_0}{\rho_{\text{ax}}} < 10.$$

When all the axons are stimulated simultaneously, the conduction velocity turns out to be strongly dependent on the coupling strength (Fig. 12). For $\beta = 1$, which produces the lowest degree of coupling, a 20% reduction of the impulse speed is obtained compared to the propagation along an isolated axon. This effect is mainly a consequence of having considered identical axons and thus identical unperturbed conduction velocities. As noted before, spikes tend to lock together in coupled fibers and to form collective pulses that propagate slowly along the nerve. In this case all the fibers get instantaneously phase-locked and a slow collective pulse is formed even at a low degree of coupling.

Figure 13 shows that at a high level of coupling there is no significant difference between stimulating the whole nerve or a large portion of it, and in both cases a slow collective pulse is generated. When a small set of fibers is stimulated, however, the conduction velocity tends to coincide with that of an isolated axon. In particular, if only 10% of the fibers of the nerve are stimulated, the conduction velocity is only 2% less than that along a single axon.

As we showed with $N = 3$, the excited fibers may induce firing in the unstimulated fibers depending on the intensity of ephaptic coupling. To explain this

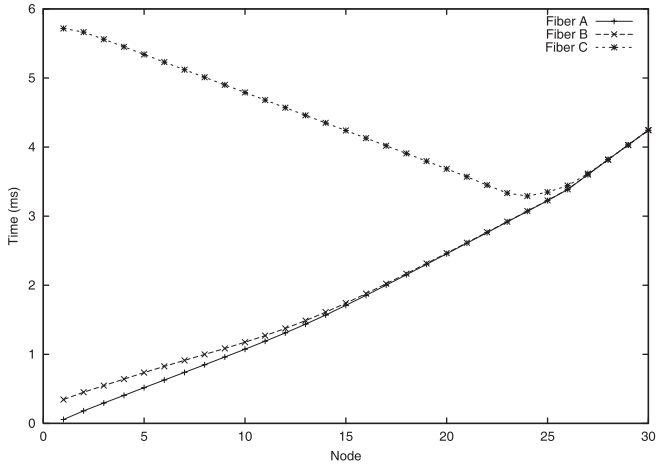

Fig. 12. Plot of conduction velocity vs. the relative extracellular resistivity, $\beta = \rho_0/\rho_{ax}$. A bundle of $N = 500$ fibers is considered; all the fibers are identical and are stimulated simultaneously. The radius of the nerve R is equal to 250 μm, and the packing ratio is kept fixed at $\gamma = 0.65$. The ephaptic interaction α is changed by varying the coefficient β. Higher coupling slows down pulse propagation. For phenomenon, we estimated the minimum number of fibers that must be stimulated to recruit all the other fibers. Simulation results show that for a high level of coupling ($\beta > 5$) the whole nerve can be driven to fire by stimulating less than one half of the fibers (Fig. 14).

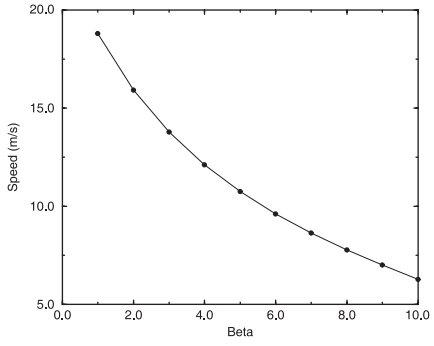

Fig. 13. Conduction velocity in a bundle of $N = 500$ fibers. The effect of the extracellular resistivity is computed with a varying number of stimulated fibers, N_s. When a large fraction of axons is stimulated, the excited fibers tend to bring all the others into conduction, and, with increasing coupling, a "collective" pulse is eventually formed that propagates slowly along the nerve. When a small set of fibers is stimulated, the CV tends to coincide with the CV of the one axon system. If, for example, only 10% of the fibers are stimulated, then the CV is only 2% less than the value of the one axon system. The reduction of CV with increasing levels of coupling is steeper when a larger fraction of axons is stimulated

Another issue we addressed is whether damaged fibers suffering a conduction block can be reexcited by the surrounding normally functioning fibers. Previous observations suggest that reexcitation is likely to occur when the whole nerve is stimulated simultaneously due to the compound effect of the propagating spikes. To test this hypothesis, a variable fraction of heavily

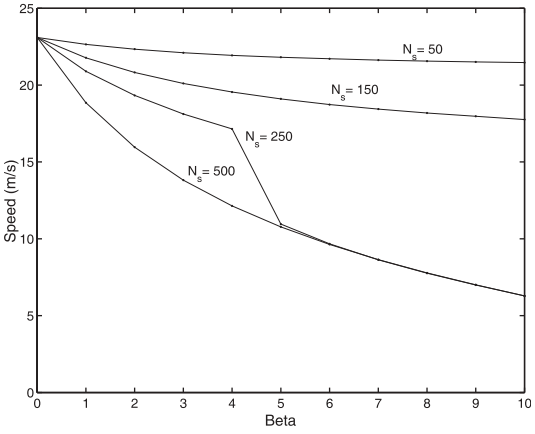

Fig. 14. The "recruiting" phenomenon in a bundle of $N = 500$ normal fibers. The minimum fraction of fibers that must be stimulated in order to excite all the other fibers in the bundle is plotted vs. $\beta = \rho_0/\rho_{ax}$. As coupling is increased, even a smaller fraction of excited fibers can trigger spiking in the whole nerve

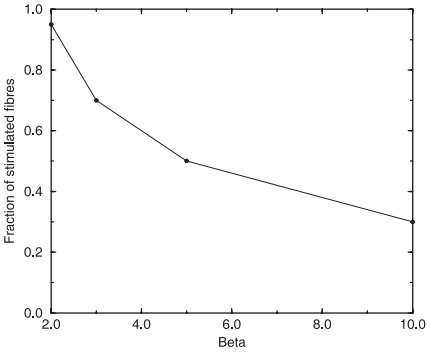

Fig. 15. Schematic drawing of a nerve bundle containing normally and segmentally myelinated fibers (longitudinal section, not to scale). A variable number of corrupted axons are considered in the simulations. The myelin sheath thickness is reduced uniformly along the same internode in all corrupted fibers. The nerve cross section S is a free parameter that defines the interaction among the fibers by means of the packing ratio $\gamma = S_{\text{free}}/S$

demyelinated fibers was considered (Fig. 15) and their response to collective stimulation was simulated at different levels of coupling.

We found that there exists a critical value $\beta_0 \simeq 3.3$ such that: (i) for $\beta < \beta_0$ no recruitment of damaged fibers into conduction is possible, (ii) for $\beta = \beta_0$ only one fiber can be recruited, and (iii) for $\beta > \beta_0$ an increasing number of fibers are recruited. In particular, for $\beta = 5$, up to 25% of the axons can be damaged without affecting collective conduction. This case is illustrated in Fig. 16, where we have traced the spike propagation along a normal and a demyelinated axon. It is worth noting that, at least for this level of coupling, reexcitement due to cross interaction occurs several nodes beyond the corrupted internode. Therefore, the spurious retrograde spikes that we observed are not directly related to demyelination but must rather be considered as a side effect of the ephaptic coupling.

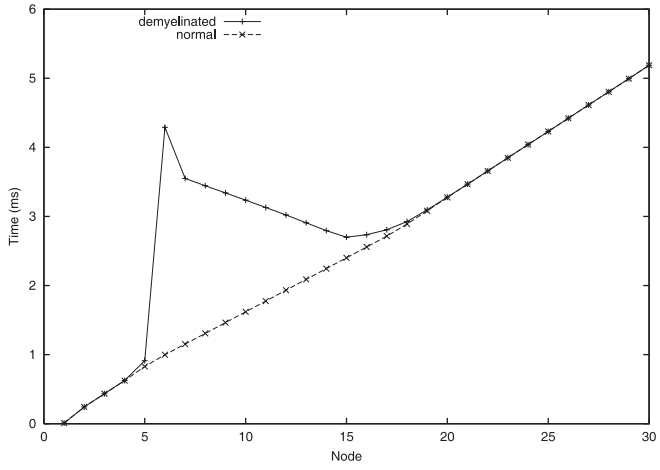

Fig. 16. Time plot of impulse propagation along normal and demyelinated fibers in a partially corrupted nerve bundle ($N_{\text{dem}}/N = 0.25$, $\beta = 5.0$). The damaged fibers are recruited into conduction through cross excitation by the undamaged fibers. A spurious back-propagating spike is generated in each damaged axon and successively absorbed by the damaged internode. We found a critical value of β, $\beta_0 \sim 3.3$ such that for $\beta < \beta_0$ no recruitment is possible; for $\beta = \beta_0$ only one fiber goes back to the normal CV, and for $\beta > \beta_0$ an increasing number of fibers can be recruited. In the case $\beta = 5$, up to 25% of axons can be damaged without changing the collective behavior

4 Discussion

Our results show the impulse conduction to be quite resistant to pathological alterations of the fiber structure such as segmental demyelination. This is consistent with what was shown by an earlier study (Koles and Rasminskiy 1972) and indicates that the actual progression of MS could remain masked with the absence of observable clinical symptoms. On the other hand, this also suggests that even a little remyelination of a corrupted fiber could be clinically advantageous. Further investigation and more detailed modelling are required to validate these hypotheses.

Computed temperature dependence would provide an explanation of why in many MS patients some of the symptoms are affected markedly by small changes in body temperature (Smith and McDonald 1999). Further, it indicates that any pharmacological factor mimicking the effect of temperature reduction on ion channel kinetics would possibly help restore function in blocked fibers.

A previous computational study demonstrated that ephaptic interaction can lead to synchronized firing in the olfactory nerve (Bokil et al. 2001), where unmyelinated axons are arranged in tightly packed bundles. Our results extend these findings to myelinated fibers. They are also consistent with the study of Binczak et al. (2001), who addressed the same phenomenon but employed a more simplified axonal model. Further examination of this issue will require a more accurate estimate of the coupling strength among axons based on morphometric analysis of the fiber size distribution inside the nerve bundles.

The formation of condensed pulse states like those shown in Sect. 3.2 has been theoretically discussed in the literature, within the context of the Fitzhugh–Nagumo approximation (Scott and Luzader 1979). In our model, we also showed that high coupling can lead to the generation of spurious spikes. This had never been shown before in such a distributed model of myelinated axons. Yet it is hard to say whether these cross-excited spikes are related to experimentally observed ectopic spikes, which might instead be due to altered excitability of the axonal membrane after complete demyelination.

Finally, if the recruiting phenomenon outlined at the end of Sect. 3.2 could be confirmed in more realistic models, this would suggest a cooperative mechanism by which damaged axons could overcome conduction block through ephaptic interaction with the surrounding undamaged fibers.

Acknowledgements. This work was funded by Serono International S.A. We thank Gianni Garotta, Luc Stoppini, Ursula Bersch, and Paola Fasani-Ghersa of the Serono Research Center for useful discussions.

Appendix

The differential system was solved by the finite difference method, applied in both x and t, with steps Δx and Δt. Denoting $x_i = i\Delta x$, $t^j = j\Delta t$, $\mathbf{U}_i^j = \left[V_1^j(i), \ldots, V_N^j(i)\right]$, where $V_k^j(i)$ is the voltage in the i-th point of the k-th fiber at the j-th time layer, this is written as a system of vector equations:

$$\begin{aligned}\widehat{\mathbf{A}}_i\mathbf{U}_{i+1}^{j+1} + \widehat{\mathbf{B}}_i\mathbf{U}_i^{j+1} + \widehat{\mathbf{C}}_i\mathbf{U}_{i-1}^{j+1} &= \mathbf{L}\left(\mathbf{U}_{i+1}^j, \mathbf{U}_i^j, \mathbf{U}_{i-1}^j\right) \\ &+ \mathbf{F}(\mathbf{U}_i^{j+1/2}, \mathbf{n}^{j+1/2}, \mathbf{m}^{j+1/2}, \mathbf{h}^{j+1/2}, \mathbf{p}^{j+1/2}), \\ &i = 2, \ldots, N_0 - 1. \end{aligned} \tag{13}$$

Here $\widehat{\mathbf{A}}_i$, $\widehat{\mathbf{B}}_i$, and $\widehat{\mathbf{C}}_i$ are $N \times N$ matrices; $\mathbf{L}$ and $\mathbf{F}$ are linear and nonlinear vector functions of the variables $\mathbf{U}_{i+1}^j, \mathbf{U}_i^j, \mathbf{U}_{i-1}^j$; and N_0 is the total number of mesh points in each fiber. Symmetric and zero conditions are set at the left and right endpoints, respectively, as in Goldman and Albus (1968).

In the calculation of the rate functions m, n, h, and p, the scheme proposed in Hines (1984) is followed. Let $V(t + \Delta t/2)$ be the potential at time $t + \Delta t/2$, assuming this is known together with the variable $y(t)$. Equation 12 can then be approximated by

$$\begin{aligned}\frac{y(t+\Delta t) - y(t)}{\Delta t Q_{10}} &= \alpha_y(V(t + \Delta t/2)) \\ &- \left[\alpha_y(V(t + \Delta t/2)) + \beta_y(V(t + \Delta t/2))\right] \\ &\times \frac{y(t+\Delta t) + y(t)}{2}. \end{aligned} \tag{14}$$

This approximation is of the second-order accuracy where the only unknown is $y(t + \Delta t)$. Collecting the terms in the expression above yields the explicit scheme

$$y(t+\Delta t)=\left[\frac{2\Delta t\alpha_y Q_{10}}{2+\Delta t Q_{10}\left(\alpha_y+\beta_y\right)}\right] + \left[\frac{2-\Delta t Q_{10}\left(\alpha_y+\beta_y\right)}{2+\Delta t Q_{10}\left(\alpha_y+\beta_y\right)}\right] y(t). \quad (15)$$

Let us assume that the values $\mathbf{m}_i^j$, $\mathbf{n}_i^j$, $\mathbf{h}_i^j$, $\mathbf{p}_i^j$, $\mathbf{U}_i^j$, $i=1,\ldots,N_0$ at the j-th time layer are known. Here $\mathbf{U}_i^j=[V_1(x_i,t^j),\ldots,V_N(x_i,t^j)]$, $\mathbf{y}_i^j=[y_1(x_i,t^j),\ldots,y_N(x_i,t^j)]$, for $y=m,n,h,p$.

The following algorithm is used to obtain the values at the next $j+1$-th time layer: (i) the right-hand sides of Eq. 13 are computed at time layer j, $\mathbf{L}(\mathbf{U}_{i+1}^j, \mathbf{U}_i^j, \mathbf{U}_{i-1}^j)+\mathbf{F}(\mathbf{U}_i^j,\mathbf{n}_i^j,\mathbf{m}_i^j,\mathbf{h}_i^j,\mathbf{p}_i^j)$; (ii) with these values, the system (13) is solved, producing the preliminary values $\widetilde{\mathbf{U}}_i^{j+1}$; (iii) the interpolated vectors of the potentials are calculated, $\widetilde{\mathbf{U}}_i^{j+1/2}=\frac{1}{2}(\widetilde{\mathbf{U}}_i^{j+1}+\mathbf{U}_i^j)$; (iv) using $\widetilde{\mathbf{U}}_i^{j+1/2}$ in Eq. 15, $\widetilde{\mathbf{m}}_i^{j+1}$, $\widetilde{\mathbf{n}}_i^{j+1}$, $\widetilde{\mathbf{h}}_i^{j+1}$, $\widetilde{\mathbf{p}}_i^{j+1}$ are computed; (v) the average values $\mathbf{y}_i^{j+1/2}=\frac{1}{2}(\mathbf{y}_i^j+\widetilde{\mathbf{y}}_i^{j+1})$ for $\mathbf{y}=\mathbf{m},\mathbf{n},\mathbf{h},\mathbf{p}$ are computed; (vi) the new right-hand sides of Eq. 13, $\mathbf{L}(\mathbf{U}_{i+1}^j,\mathbf{U}_i^j,\mathbf{U}_{i-1}^j)+\mathbf{F}(\widetilde{\mathbf{U}}_i^{j+1/2},\widetilde{\mathbf{n}}_i^{j+1/2},\widetilde{\mathbf{m}}_i^{j+1/2},\widetilde{\mathbf{h}}_i^{j+1/2},\widetilde{\mathbf{p}}_i^{j+1/2})$ are derived; (vii) the final values of $\mathbf{U}_i^{j+1}$ are obtained solving Eq. 13 with these new right-hand sides; (viii) the average values $\mathbf{U}_i^{j+1/2}=\frac{1}{2}(\mathbf{U}_i^{j+1}+\mathbf{U}_i^j)$ are computed; (ix) the final values $\mathbf{m}_i^{j+1}$, $\mathbf{n}_i^{j+1}$, $\mathbf{h}_i^{j+1}$, $\mathbf{p}_i^{j+1}$ at the new time layer are computed using $\mathbf{U}_i^{j+1/2}$ in formulae similar to Eq. 15, and the algorithm is closed.

References

Baker M, Bostock H (1992) Ectopic activity in demyelinated spinal root axons of the rat. J Physiol Lond 451: 539–552

Binczak S, Eilbeck JC, Scott AC (2001) Ephaptic coupling of myelinated nerve fibres. Physica D 148: 159–174

Bokil H, Laaris N, Blinder K, Ennis M, Keller A (2001) Ephaptic interactions in the mammalian olfactory system. J Neurosci 21: 1–5

Brill MH, Waxman SG, Moore JW, Joyner RW (1977) Conduction velocity and spike configuration in myelinated fibers: computed dependence on internode distance. J Neurol Neurosurg Psychiatry 40: 769–774

Frankenhaeuser B, Huxley AF (1964) The action potential in the myelinated nerve fibre of *Xenopus Laevis* as computed on the basis of the voltage clamp data. J Physiol Lond 171: 302–315

Goldman L, Albus JS (1968) Computation of impulse conduction in myelinated fibres; theoretical basis of the velocity–diameter relation. Biophys J 8: 596–607

Hines M (1984) Efficient computations of branched nerve equations. Int J Biomed Comput 15: 69–76

Hodgkin AL, Huxley AF (1952) A quantitative description of membrane current and its application to conduction and excitation in nerve. J Physiol Lond 117: 500–544

Koles ZJ, Rasminsky M (1972) A computer simulation of conduction in demyelinated nerve fibres. J Physiol Lond 227: 351–364

Markin VS (1970a) Electrical interactions of parallel nonmyelinated fibres: I. Change in excitability of the adjacent fiber. Biofizika 15: 120–128

Markin VS (1970b) Electrical interactions of parallel nonmyelinated fibres: II. Collective conduction of impulses. Biofizika 15: 681–689

Matthews WB (1975) Paroxysmal symptoms in MS. J Neurol Neurosurg Ps 38: 619–623

Nygren A, Halter JA (1999) A general approach to modeling conduction and concentration dynamics in excitable cells of concentric cylindrical geometry. J Theor Biol 199: 329–358

Scott AC, Luzader SD (1979) Coupled solitary waves in neurophysics. Phys Scripta 20: 395–401

Smith R, Koles Z (1970) Myelinated nerve fibers: computed effect of myelin thickness conduction velocity. Am J Physiol 219: 1256–1258

Smith KJ, McDonald WI (1980) Spontaneous and evoked electrical discharges from a central demyelinating lesion. Phil Trans R Soc Lond B 354: 1649–1673

Smith KJ, McDonald WI (1982) Spontaneous and evoked electrical activity due to central demyelinating lesion. Nature 286: 154–155

Smith KJ, McDonald WI (1999) The pathophysiology of multiple sclerosis: the mechanism underlying the production of symptoms and natural history of the disease. Phil Trans R Soc Lond B 354: 1649–1673

Stephanova D (1989) Conduction along myelinated and demyelinated nerve fibers during the recovery cycle: model investigations. Biol Cybern 62: 83–87

Tasaki I (1953) Nervous transmission. Thomas, Springfield, IL

Tuckwell Henry C (1993) Voltage clump calculations for mylinated and demyelinated axons. Eur Biophys J 22: 71–77

Waxman SG (1977) Conduction in myelinated, unmyelinated and demyelinated fibers. Arch Neurol 34: 585–589

Waxman SG, Brill MH (1978) Conduction through demyelinated plaques in multiple sclerosis: computer simulations of facilitation by short internode. J Neurol Neurosurg Psychiatry 41: 408–416